Chapter 4
Multistability in Lasers

Abstract Lasers are nonlinear optical devices where multistability has been extensively studied. That is why in this book we pay special attention to multistability in lasers and devote an entire chapter to this topic. After introducing the reader to the main principles of laser dynamics, we start our consideration of laser multistability with the so-called *optical bistability* or the coexistence of two different outputs of the laser light transmitted through an optical cavity filled with a resonant medium. In fact, an optical bistable system is the passive counterpart of a laser. The phenomenon of optical bistablity theoretically predicted by Szoke et al. [1] was observed in the experiments of Gibbs and colleagues [2]. Their findings stimulated intensive theoretical and experimental research in this direction. It was only in the early 1980s that multistability became a noticeable phenomenon in laser physics. Here, after a short excursion back to the history of nonlinear laser dynamics, we will describe the main features of optical bistability and generalized multistability in laser systems of different types.

4.1 Laser as a Nonlinear Dynamical System

4.1.1 History of Laser Dynamics

A laser is an electro-optical device that produces coherent radiation. The term "laser" has been widely used since about 1965. LASER is the abbreviation for the word "Light Amplification by Stimulated Emission of Radiation." At first it was called an "optical quantum generator" or "optical MASER" (Microwave Amplification by Stimulated Emission of Radiation). The first masers were created in 1953–1954 by Russian physicists Nikolai G. Basov and Alexander M. Prokhorov and independently by American physicist Charles Townes. In 1955, Prokhorov and Basov proposed optical pumping of a multilevel system as a method for obtaining a population inversion, which later became one of the main methods of laser pumping. In 1964, Townes, Basov and Prokhorov shared the Nobel Prize in Physics "*For fundamental work in the field of quantum electronics, which led to the creation of oscillators and amplifiers*

A. N. Pisarchik and A. E. Hramov, *Multistability in Physical and Living Systems*,
Springer Series in Synergetics, https://doi.org/10.1007/978-3-030-98396-3_4

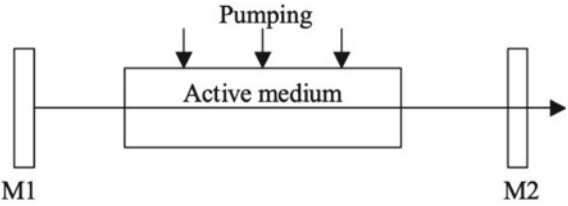

Fig. 4.1 A laser construction with a Fabry–Pérot cavity. M1 and M2 are full reflective and semitransparent mirrors, respectively

based on the maser-laser principle." Indeed, the laser has revolutionized optical technology and has had a far-reaching influence in various fields of science and life in general.

As a rule, a laser consists of an amplifying (active) medium with inverted population and a cavity formed by two mirrors M1 and M2, which form a Fabry–Pérot resonator confining light between the mirrors (Fig. 4.1). Instead of flat mirrors, concave mirrors, diffraction gratings or Bragg reflectors are also used, and sometimes an optical cavity with more than two mirrors is utilized. The active medium is excited from an external energy source (electrical, chemical, or optical). The active medium plays an important role in the light amplification by population inversion and stimulated emission. There are many types of active media that can be used to produce lasing at different wavelengths. Thus, we can say that a laser is a nonlinear optical oscillator or an amplifier of light waves.

Since its discovery and until the mid-1960s, the laser was thought as a "stable" device whose instability was treated as a consequence of mechanical vibration or bad cavity alignment. Nonlinear laser dynamics was conceived by Russian physicists Grazyuk and Oraevsky [3], who found that the coherent single-mode laser equations, which are a simplified version of the more modern Maxwell–Bloch theory, predict instabilities and stable oscillations without well-defined mathematical conditions that do not affect the unsaturated gain of the active medium in the cavity and the rate of atomic relaxation.

By coherent laser equations, we mean a theory based on the existence of an interaction between an optical wave and atomic dipoles, which assumes a relationship between an optical wave and macroscopic polarization in accordance with Maxwell's electrodynamics. In numerical studies of equations describing the simplest (uniformly broadened, single-mode, traveling wave, resonantly tuned) laser, they found a non-stationary solution consisting of pulses that irregularly vary in time. At the time, they even used the term "chaotic" to describe this irregular, pulsating behavior.

Laser dynamics was in its infancy for over a decade until the mid-1970s, when the German theoretical physicist Hermann Haken, based on the isomorphism of the laser with Lorentz equations, came to the conclusion that lasers should exhibit nonperiodic pulses. However, in the early 1980s, many researchers did not believe that the Lorentz–Haken instability was inherent in real laser systems. They thought it was just an academic curiosity invented by theoreticians far remote from the daily reality of experimental laser physics. Nevertheless, chaos and multistability were soon discovered in lasers giving rise to a new research field named *Nonlinear Laser Dynamics*.

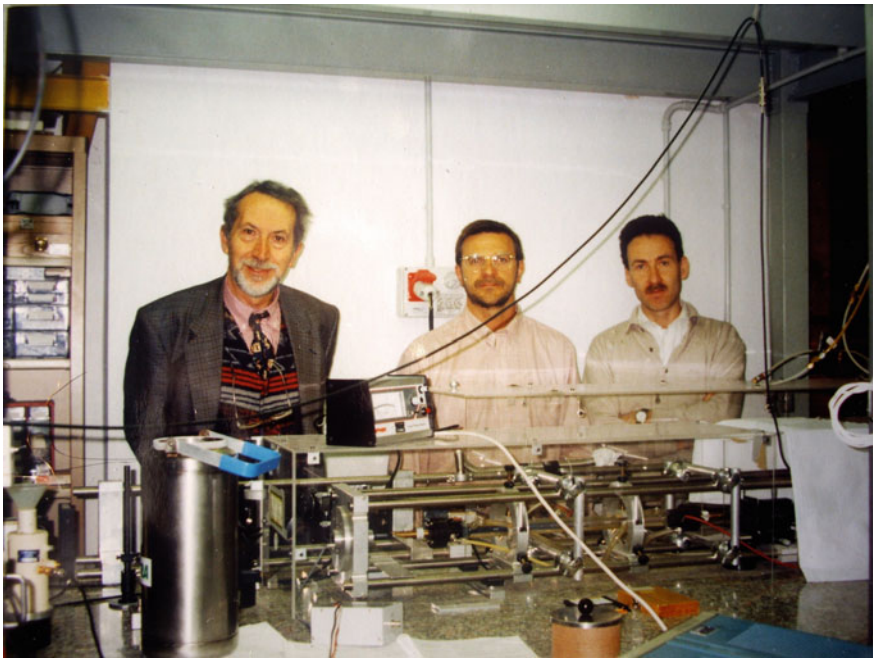

Fig. 4.2 Tito Arecchi (left), Alexander Pisarchik (center), and Riccardo Meucci (right) behind the CO_2 laser setup at the National Institute of Applied Optics (Istituto Nazionale di Ottica Applicata). Florence, Italy, April 1999

The first clear experimental evidence of multistability in laser systems was demonstrated in 1982 by the group of Tito Arecchi [4], who found the coexistence of two oscillatory regimes in a loss-modulated CO_2 laser (see Fig. 4.2). They called this phenomenon *generalized multistability* to distinguish it from "optical bistability" meaning the coexistence of two stable steady states. At the same year, bistability was experimentally observed in a multimode infrared He–Ne laser by the group of Carl Weiss [5]. Later, Brun and colleagues [6] observed the coexistence of periodic and chaotic pulsations in a nuclear spin-flip laser. Since then, the coexistence of various attractors has been found in other types of lasers, including solid-state lasers with intracavity second harmonic generation [7], semiconductor [8, 9], and fiber lasers [10, 11]. These results sharpened the concept of lasers as "unstable" systems and stimulated new experimental and theoretical research.

From the very beginning of the laser industry, stabilization of irregular fluctuations in the intensity of laser radiation has been an important problem. However, instability and chaos are inherent in the nonlinear nature of laser systems with three or more degrees of freedom. For example, in multimode lasers or in lasers with nonlinear intracavity devices, nonlinear coupling between modes can lead to instability and multistability of the laser intensity. It is quite obvious that the irregular behavior of such lasers is an undesirable situation for many practical applications. Scientists

faced this problem first in a diode-pumped Nd:YAG (neodymium-doped yttrium-aluminum garnet) (1.06 μm) with intracavity second harmonic generation (green light) and thus called "green problem" [7]. Several theoretical and experimental works have been devoted to avoiding such irregular behavior and switching between coexisting states [12].

A special type of multistability, *spatial multistability* was also found in lasers in the form of coexisting transverse spatial patterns which appear due to the interaction of cavity modes. In order to describe spatial multistability in optical patterns, Brambilla et al. [13] argued a general connection between laser physics and hydrodynamics, reformulating the equations of laser dynamics in the form as the equations of hydrodynamics for a compressible fluid in accordance with the law of conservation of mass and the Bernoulli equation. Two-dimensional optical patterns can also result from synchronization of several wave vectors of different lengths and orientations [14]. Multistability of optical structures can be useful for information processing, associative memory, and pattern recognition [15].

4.1.2 Dynamical Classification of Lasers

Lasers are usually classified according to the active medium providing optical amplification. This material largely determines the properties of the laser: operating mode (pulsed or continuous), radiation wavelength, output power/energy, and coherence properties. Gases, liquids and solids can provide optical amplification when properly excited.

Another classification of lasers is based on timescale considerations. This classification was introduced by Arecchi et al. [16], who opened a new view of lasers as dynamical systems and can be regarded as one of the most important advances in laser dynamics. Similar to other nonlinear devices, the laser can be modeled by rate equations. In particular, many lasers are described by three differential equations. Three relevant variables (field, population, and polarization) decay at different time scales, which are given by the corresponding relaxation rates (κ, $\gamma_\parallel$, and $\gamma_\perp$). If one of these constants is larger compared to the others, the corresponding variables are rapidly weakened and therefore adjust adiabatically to the other variables. Thus, the number of equations describing the laser can be reduced. More precisely, single-mode lasers are named classes A, B, and C depending on whether the laser dynamics is ruled, after appropriate adiabatic elimination of fast variables, by one, two, or three equations, respectively.

Thus, the following laser classification is now widely accepted.

Class A (for example, He-Ne, Ar, Kr, dye lasers): $\gamma_\perp \simeq \gamma_\parallel \gg \kappa$. The dynamics of these lasers are modeled by only one nonlinear field equation resulting in a stable coherent emission.

Class B (for example, ruby, Nd:YAG, CO, CO_2, semiconductor, fiber lasers): $\gamma_\perp \gg \kappa \leq \gamma_\parallel$. Only polarization is adiabatically eliminated so that the dynamics is

ruled by two rate equations for field and population that allows for damped oscillations (relaxation oscillations) of the energy between field and inversion.

Class C (for example, He-Cd, He-Xe, far-infrared gas lasers): $\gamma_\perp \simeq \kappa \simeq \gamma_\parallel$. The complete set of three rate equations has to be used, and therefore chaos is possible.

Thus, chaotic dynamics and multistability are impossible in class A and B lasers without adding additional degrees of freedom, which can be introduced using either an external action (for example, parametric modulation or injection of external light), an intracavity nonlinear medium (saturable absorber), a feedback, or in a bidirectional ring cavity.

In general, a small change in one or more laser parameters causes small (smooth) changes in the laser output, so that the laser is considered "structurally stable". However, for some specific values of the parameters, one of the solutions (or attractors) can undergo a strong qualitative change (bifurcation), and the laser is considered "structurally unstable". Very often, when the control parameter is changed and a bifurcation appears at a certain critical value, the laser undergoes a sequence of new bifurcations at higher values of the parameter. Each new attractor that appears in the chain of bifurcations is usually more complex than the previous one and eventually becomes chaotic. Such a sequence of bifurcations is called "the road (or route) to chaos." The number of types of routes to chaos in lasers is large and exactly unknown, but it has been observed that some of them appear very often, and for this reason they are called "scenarios." The most often scenarios are the Feigenbaum (or period-doubling), Ruelle–Takens–Newhouse (or quasiperiodicity), and intermittency (types I–III, Pomeau–Manneville, on-off, crisis-induced) routes to chaos.

4.2 Multistability in Optical Systems

In this section, we describe different types of multistability in optical and laser systems, in particular, optical bistability, spatial multistability, and polarization multistability.

4.2.1 Optical Bistability

Optical bistability is the general name for a number of static and dynamic phenomena that arise from the interaction of optical nonlinearity and feedback. The comprehensive reviews can be found in Refs. [17–19].

An optically bistable system is a system that exhibits two stable output signal states at the same input radiation intensity. The simplest example of such a device consists of a Fabry–Perot cavity filled with a nonlinear media whose refractive index depends on the radiation intensity I as $n = n_0 + n_2 I$ (n_0 and n_2 being constants), as illustrated in the left panel in Fig. 4.3.

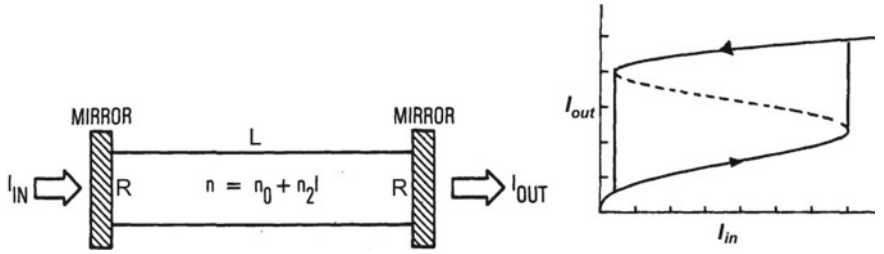

Fig. 4.3 (Left) Fabry–Perot interferometer of length L and mirror reflectivity R. I_{in} and I_{out} are incident and transmitted intensities. (Right) Characteristic curve of the optical cavity showing bistability. As the input intensity I_{in} varies, the transmitted intensity I_{out} exhibits a hysteresis cycle. The dashed line indicates unstable equilibria

The transfer function of the Fabry–Perot interferometer, that is the ratio of the output intensity to the input intensity, as known to depend on the radiation wavelength λ as [20]

$$\frac{I_{in}}{I_{out}} = \frac{1}{1 + F \sin^2(\Phi/2)}, \tag{4.1}$$

where $F = 4R/(1 - R)^2$ is the cavity finesse and

$$\Phi = 2\pi n_o \frac{L}{\lambda} + \frac{4\pi n_2 L}{\lambda} I_{in} \tag{4.2}$$

is the round-trip phase shift.

An increase in the input intensity causes a decrease in the effective wavelength and, accordingly, an increase in the transmission. As a result, the cavity optical length nL is a periodic function of I. One can see in the right panel in Fig. 4.3 that the transfer function displays a hysteresis behavior, i.e. there is a region of input intensities for which the output intensity has two stable values for a given input intensity. The two values represent high and low transmitting levels or states. This is a typical example of bistability which arises in saddle-node bifurcations (see Sect. 2.1.2).

Miller and colleagues [21] were the first to experimentally observe optical bistability in InSb at 1895 cm^{-1} near the absorption edge at 5 K. The nonlinear term in Eq. 4.2 indicates that the longer the cavity, the lower the intensity required for these effects, but if the cavity is too long, then linear absorption becomes important, and this leads to a decrease in efficiency, and therefore bistability may not occur.

Bistable optical systems usually contain either a saturable absorber or a nonlinear dispersive medium and an optical feedback loop. However, aerosols and suspensions of dielectric nanoparticles (soft matter) can also be used as nonlinear media, since in this case nonlinear effects can be observed at very low power levels [22].

Pobegalov et al. [23] discovered a new type of optical bistability obtained with low-power lasers and using defocusing nonlinearity in nanoparticle suspensions. The ability to use light to control properties of nanosuspensions at a mesoscopic

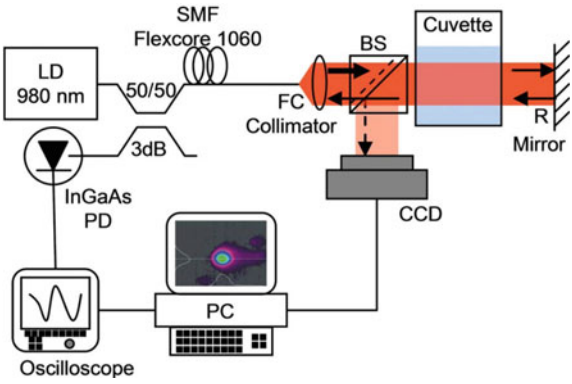

Fig. 4.4 Experimental setup for observation of low-power optical bistability in the optoliquid system. It includes a fiber pigtailed semiconductor laser diode (LD) with nonlinear incoherent optical feedback. To visualize coexisting optical patterns, a CCD camera is used. Reprinted with permission from [23] ©2014 The Optical Society

level makes such a system very attractive for the rapidly developing field of optofluidics [24, 25] which combines microfluids and photonics, creating new possibilities for optical information processing. In addition, low-power optoliquid systems are especially promising for biomedical applications, as they can provide nondestructive inspection and verification of biological objects. Using a semiconductor laser diode operating near the threshold at a 980-nm wavelength and a colloidal solution of LaF_3:Er and Yb nanocrystals with resonant optical absorption at the same wavelength, optical switching of several milliwatts was obtained. Figure 4.4 shows the experimental setup for studying optical bistability.

The bifurcation diagram of the laser intensity at the center of the laser beam is presented in Fig. 4.5a. It displays hysteresis with respect to the pump current. Optical bistability is observed as switching between high-power and low-power states of the photodetector signal, accompanied by a radical change in the cross-section profile of the optical feedback beam, i.e. the transition from a simple bell-shaped profile to an annular one, meaning, respectively, high-power and low-power states illustrated in Fig. 4.5b,c. In the hysteresis range, two different laser beam profiles coexist and can be found by changing the direction of the pump current change. The origin of optical bistability relies on the incoherent optical feedback and thermal defocusing nonlinear optical response of the nanosuspension.

The change in the beam profile can also be interpreted as spatial bistability caused by spontaneous emission of four-wave mixing in the off-axis direction. The hysteresis appears due to a special operation mode of the laser with incoherent optical feedback.

4.2.2 Spatial Multistability

Spatial multistability is a specific type of multistability which reveals itself as the coexistence of different patterns in space for the same set of system parameters. Spatial bistability, was first experimentally observed in 1990 in a helium-neon (He-Ne)

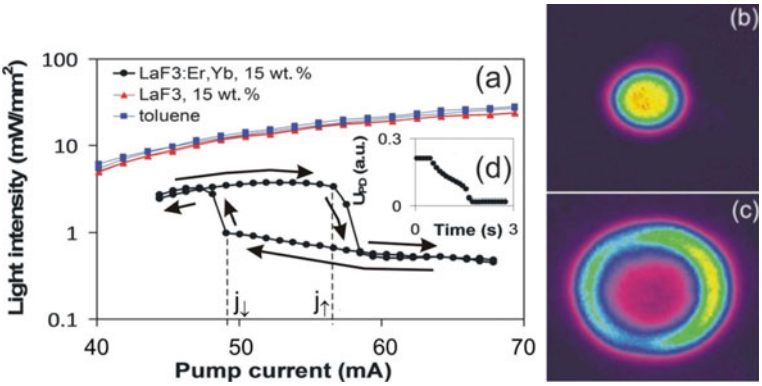

Fig. 4.5 Optical bistability in a laser system. **a** Output light intensity at the beam center at the CCD camera as a function of laser-diode current for pure toluene (squares). **b**, **c** Coexisting output beam profiles in high- and low-intensity states. Adapted from [23]

laser oscillating in the $\mathrm{TEM}^{\star}_{01}$ hybrid optical-resonator mode [26]. One year later, Brambilla and colleagues [13] reported on their findings of the coexistence of three and four different pattern configurations of the laser field. Then, this phenomenon was observed in other nonlinear systems, such as cell replication models [27], continuous stirred tank reactors [28], protein-protein interactions [29], reaction-diffusion systems [28, 30, 31], ecosystems [32–34], planar exciton-polariton condensates [35], multimode vertical-cavity lasers [36], and arrays of graphene [37].

We can distinguish two types of spatial multistability conventionally called *exogenous* and *endogenous*. The former type is referred to the case when coexisting patterns are caused by an external source, while the latter type results from synchronization of coupled systems. For example, the coexistence of different laser modes caused by a laser beam passed through a Fabry–Perot resonator belongs to the exogenous type of spatial multistability. Another example of exogenous spatial multistability is the coexistence of different patterns in brain imaging of electrical or magnetic activity induced by ambiguous stimuli (see Chap. 8). Examples of endogenous spatial multistability are multistable spatial dynamics of reaction-diffusion systems and multistability in cell replication. In addition, spatial multistability in complex networks can manifest itself as the coexistence of synchronous and asynchronous oscillations. Such a behavior referred to as *multistable chimeras* [38, 39] will be described in Chap. 6.

The first example demonstrating that laser dynamics can be characterized by the transverse structure of the laser field was given by Lugiato and Milani [40]. They showed that for a fixed Gaussian transverse distribution of the intensity of laser modes in a uniformly broadened laser, there are no "bad-cavity" or "good-cavity" single-mode laser instabilities. In other words, neither single-mode instabilities nor instabilities with the participation of several longitudinal modes arise.

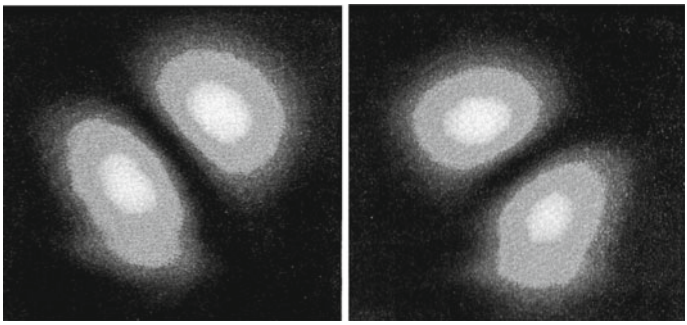

Fig. 4.6 Coexisting TEM_{01} and TEM_{10} laser modes. Reprinted with permission from [26] ©1990 The Optical Society

Tamm and Weiss [26] were the first who experimentally observed spatial bistability. It was achieved with a small screen placed at the center of the He–Ne laser beam waist. When the laser is tuned to cavity modes with zero intensity at the center, it usually emits in TEM_{01} or TEM_{10} mode, or both, as illustrated in Fig. 4.6. By moving the point of the absorber, it is possible to make the intensities of both modes more or less equal. At the same time, switching between these two modes occur due to inherent laser noise.

4.2.3 Polarization Multistability

Due to a vector character of electromagnetic field **E**, there is a phase difference between two components E_x and E_y of output light passed through a nonlinear medium. The coexistence of two laser beams with ortogonal polarization was first observed by Chen and Liu [41] in an edge-emiting semiconductor laser. This type of optical bistability was revealed near the polarization transition temperature with a hysteresis in the laser power versus the injection current. Later, polarization bistability was also found and extensively studied in vertical cavity surface lasers (VCSELs) [42].

VCSELs are widely used as light sources in optoelectronic devices, optical communications and measuring systems, in particular, in communication systems for data transmission, laser printers, autodyne interferometry, atomic clocks, various spectroscopic schemes, etc. [43]. VCSELs have a number of advantages over other types of semiconductor lasers. In particular, they are relatively cheap, the laser beam is of a high quality, and the lasing threshold is low. In addition, these lasers provide broadband modulation that is important for communication. Extensive efforts were concentrated on the stabilization of polarization that is important for the application of these lasers in a polarization-sensitive equipment, such as, magneto-optic

disks and coherent detection systems. On the other hand, fast switching between two orthogonal polarization states can be useful for applications in all-optical switching and optical memory.

The physical mechanism underlying polarization multistabillity in VCSEL lies in the fact that the guided fundamental laser mode does not have azimuthal changes and, therefore, the distribution of the optical field depends only on the lateral position. Since a preferential axis of symmetry in the circular cross-section does not exist, the electric field can be directed so that it is everywhere parallel to one of the arbitrary pair of orthogonal directions. Moreover, the two orthogonally polarized beams are amplified in the active layer of an isotropic quantum well active, so that the two polarization states become nearly degenerated. Dispersive bistability is caused by gain saturation that can be obtained through the input Y-polarized beam when the optical gain is depleted during the amplification of the Y-polarized beam, and hence X-polarized mode is suppresses. At the same time, the amplification of the Y-polarized mode is accompanied by a decrease in carrier concentration, which in turn causes an increase in the refractive index of the active medium. Dispersive bistability in both X- and Y- polarized outputs appears if the wavelength of the injected Y-polarized light is slightly larger than the wavelength of the Y-polarized light in the cavity without external optical injection. It was found that the dispersive bistability and gain saturation powers of the X- and Y-polarized models depend on the temperature, dispersion, and the VCSEL structure.

As a rule, bistability in single-mode VCSEL lasers is observed as spontaneous polarization switching during the scanning of the pump current that leads to hysteresis. Multimodal VCSELs behave in a similar way, however, several polarization states can coexist at high pump currents, namely, three [44], four, and five [45] polarization states were observed. In addition, two types of multistability (polarization and spatial) simultaneously exist in this laser [36].

Figure 4.7 shows the experimentally observed coexisting spatial patterns of the VCSEL intensity corresponding to different polarization states which were obtained for the same parameters using different initial conditions. The measurements were performed with a 852-nm VCSEL. The collimated laser beam was split into two equal beams. One was recorded by a photodiode to analyze the integrated intensity, and another passed through a half-wave plate and split by a Glan prism into two orthogonal polarization components. One of these components was recorded by a CCD camera to analyze spatial beam profile, while another component was recorded by a second photodiode to analyze laser dynamics of a particular polarization. A spatial beam profile was recorded by the CCD camera.

As seen from Fig. 4.7, polarization multistability manifests itself in the form of coexisting spatial structures or, in other words, different distributions of laser radiation intensity in the beam cross-section at the same parameters. The coexistence of two, three, and four spatial distributions of the laser intensity were experimentally observed in this laser. Thus, polarization multistability leads to spatial multistability in the integral laser intensity.

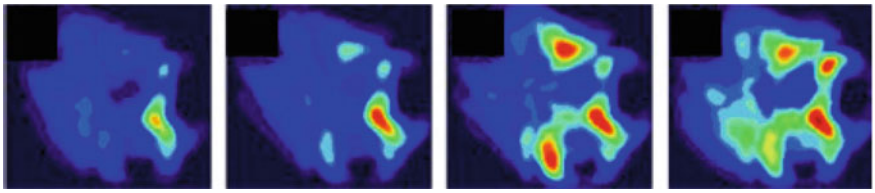

Fig. 4.7 Four coexisting spatial distributions of the VCSEL intensity corresponding to different polarization states. Based on data from [46]

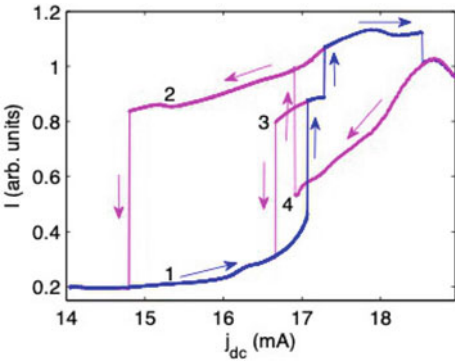

Fig. 4.8 Laser intensity of different polarization versus dc pump current. The arrows show the directions of the current changes and switches between different polarization states. The hysteresis is obtained by increasing and decreasing pump currents starting from different initial conditions

Polarization multistability is clearly seen in Fig. 4.8 which displays the laser intensity when the bias current is slowly increased and decreased. One can see that for certain currents two, three, and even four polarization states coexist.

The theoretical analysis of polarization bistability in VECSELs and conditions necessary for its occurrence were derived by Yu [47]. In particular, he substantiated that (i) the input power required to achieve polarization bistability depends on the matching between the gain and the resonator mode. When the gain is blue-shifted relative to the resonator mode, then the hysteresis loops are shifted towards the low-power side of the input Y-polarized light. However, the opposite situation occurs for the red-shift alignment. (ii) Self-heating effect is minimized for the blue-shifted alignment because the low injection power is required for bistability. (iii) The reflectivity of Bragg reflectors affects the bistable performance of the VCSEL. Devices with low reflectivity require low input power to achieve bistability, but the strength of the coupling between the injected light and the active layer is reduced. Therefore, the use of polarization bistability in VCSELs for all-optical switching and optical memory requires a blue-shifted gain relative to the cavity mode to reduce input power and self-heating.

It should be noted that polarization bistability was found not only in semiconductor laser, but also in liquid crystals in the Fabry–Pérot optical resonator [48–50], counter-propagating laser beams through a nonlinear medium [51], and in a He–Ne laser with saturable absorber [52].

4.3 Multistability in CO_2 Lasers

The CO_2 laser with harmonic modulation of cavity losses was the first laser system where the coexistence of different periodic orbits was observed [4]. Using an intracavity electro-optical modulator, Arrecchi and colleagues found that at certain modulation frequencies the laser operated either in a period-3 or in a period-4 regime. The coexistence of these regimes was found in the average power spectrum of the laser output intensity, where the both subharmonic frequencies were observed, as illustrated in Fig. 4.9. The switching between the two periodic orbits was explained by the influence of internal laser noise.

Later, bistability in a CO_2 laser was observed under harmonic modulation of the cavity optical length [53], optical injection [54, 55], delayed feedback [56], pump current modulation, and cavity detuning [57].

4.3.1 Loss-Modulated CO_2 Laser

A CO_2 laser belongs to class-B lasers, i.e. the polarization term can be adiabatically eliminated so that the laser can be described by two rate equations, for the laser intensity and for population inversion. Nevertheless, it is possible to observe nonlinear dynamical effects in this class of lasers, including chaos and multistbility if we add an additional degree of freedom in the form of external modulation, intracavity saturable absorber, or feedback.

The simplest two-level model of the active medium of a single-mode CO_2 laser contains two dimensionless variables that describe radiation power density u in the cavity and gain y in the active medium [58, 59]:

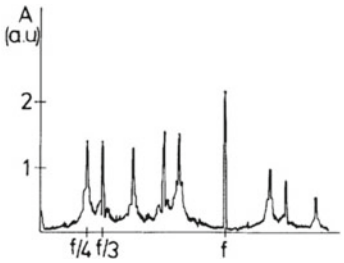

Fig. 4.9 Experimental averaged power spectrum of the CO_2 laser intensity demonstrating the coexistence of period-3 and period-4 regimes. $f/3$ and $f/4$ are subharmonics of the modulation frequency f

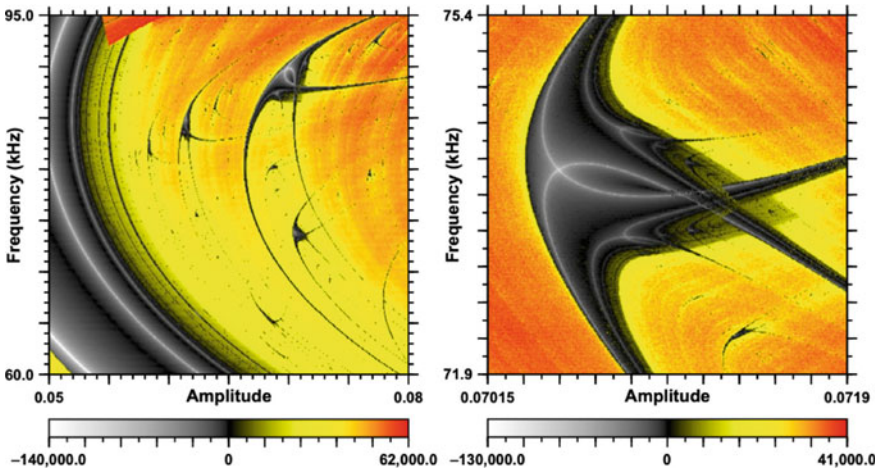

Fig. 4.10 Lyapunov exponents in the CO_2 laser (Eq. 4.3) with loss modulation (Eq. 4.4) in the space of modulation amplitude k_d and frequency f_d. The right diagram is the enlarged area of the left diagram. Negative exponents (in grey) represent periodic regimes, while positive exponents (in colors) indicate the regime of chaotic oscillations. Reprinted from [60] ©2016 with permission from Elsevier

$$\begin{aligned} \dot{u} &= \tau^{-1}(y-k)u, \\ \dot{y} &= (y_0 - y)\gamma - uy, \end{aligned} \tag{4.3}$$

where y_0 is unsaturated gain, τ is half of the round-trip time of light in the laser cavity, γ is the gain decay rate, and k is the total cavity losses.

Complex dynamics in a class-B laser appears when cavity losses are periodically modulated as follows

$$k(t) = k_0(1 + k_d \cos(2\pi f_d t)), \tag{4.4}$$

where k_0 is the constant part of the losses, and k_d and f_d are the driving amplitude and frequency.

For parameter values $\tau = 3.5 \times 10^9$ s, $\gamma = 1.978 \times 10^5$ s^{-1}, $y_0 = 0.175$, and $k_0 = 0.1731$ and using a and f as control parameters, the phase-space structure of the system stability (in terms of Lyapunov exponents) exhibits so-called *shrimps* illustrated in Fig. 4.10. The shrimps represent a complex structure consisting of a doubly infinite sequence of period-doubling bifurcations, followed by chaotic oscillations.

Figure 4.11 shows the bifurcation diagram of peak values of u versus driving amplitude f_d obtained by numerical simulations of Eqs. 4.3 and 4.4 using random initial conditions [61]. One can see three branches (T, 2T, and 3T) which correspond to different attractors starting from period-1, period-2, and period-3 orbits. As k_d is increased, these orbits undergo period-doubling bifurcations followed by crisis and chaos. For certain values of k_d, there is bistability and tristability.

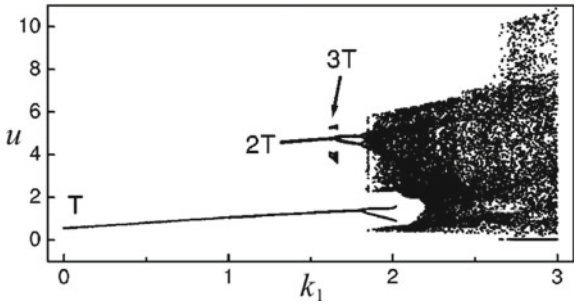

Fig. 4.11 Bifurcation diagram of the peak values of laser density u as a function of the driving amplitude k_d. T, 2T, and 3T are stable branches of the period-1, -2, and -3 orbits. $y_0 = 0.1805$, $f_d = 112$ kHz

4.3.2 Targeting Attractors by Short Pulses

To find coexisting attractors in a loss-modulated CO_2 laser, Chizhevsky and colleagues [62, 63] applied a short (as compared to characteristic times in the system) perturbation to the laser field. In fact, the method is equivalent to the Monte Carlo method (see Sect. 2.3.2), when the initial condition is randomly changed. In this case, the laser turns off for a very short time, and then turns on again, but under different initial condition and, therefore, can be instantly sent to the basin of attraction of another coexisting attractor. An important advantage of this method is that it can easily be used in experiments, since it does not require any prior knowledge of the model. Since the pulse is very short, no significant changes in the laser parameters occur during the switching time, so that the global structure of attractors in phase space remains unchanged. In addition, switching with short pulses is a well-controlled deterministic process, so that the laser response is reproduced with a very high accuracy.

A scheme of the experimental setup for identifying coexisting attractors in a CO_2 laser is drawn in Fig. 4.12. A 15-ns pulse of a Nd^{3+}:YAG laser is applied to a GaAs plate inside the cavity of a single-mode cw CO_2 laser, which leads to an increase in the concentration of nonequilibrium carriers, which, in turn, increases the absorption of CO_2 laser radiation. As a result, the CO_2 laser stops generating radiation for a short pulse time. The back edge of the induced losses is determined by the lifetime of nonequilibrium charge carriers in GaAs, which does not exceed 300 ns. Both time constants are much shorter than the period of loss modulation by an acousto-optic modulator based on a Thallium Halogenide (KRS-5) crystal, exceeding 10 μs.

To obtain a particular coexisting attractor, the amplitude and phase of the Nd:YAG laser pulse must be matched with the phase of loss modulation of the CO_2 laser. For this, the following procedure is used. For a fixed pulse amplitude, its phase (i.e. its delivery time) is shifted relative to the phase of modulation of the CO_2 laser losses. By shifting the pulse phase, all coexisting states can be found.

Using this approach, the coexistence of four periodic orbits was revealed in the loss-modulated CO_2 laser, namely, period 1 (T), period 3 (3T), period 4 (4T), and period 5 (5T), for the same set of the laser parameters. The switching between different coexisting attractors is illustrated with the oscilloscope recordings in the left

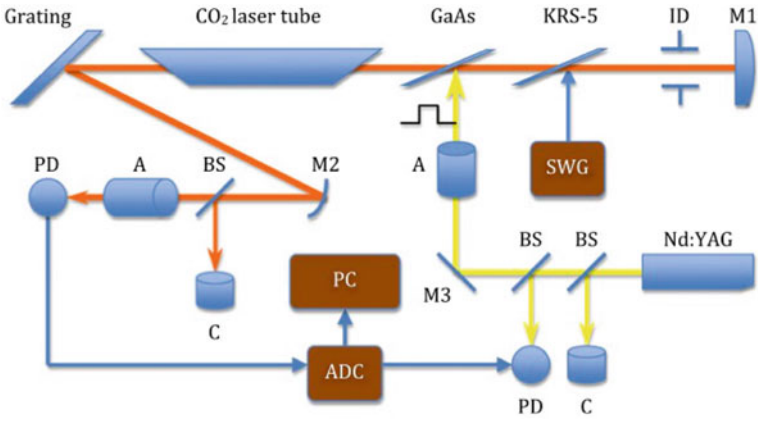

Fig. 4.12 Experimental setup for searching coexisting attractors in a loss-modulated CO_2 laser by an external short-pulsed perturbation from a Nd:YAG laser. M1, M2, and M3 are a totally reflecting mirror. The cavity losses are modulated by a harmonic signal applied from a sine wave generator (SWG) to an acousto-optical modulator (KRS-5). Switching between coexisting attractors is realized by short pulses of the Nd^{3+}:YAG laser applied to a GaAs plate. ID is an iris diaphragm, BS are beam splitters, PD are photodetectors, A are optical attenuators, C are calorimeters, ADC is an analog-to-digital converter, and PS is a computer

panel in Fig. 4.13. Multistability is clearly seen in the experimentally reconstructed bifurcation diagrams of the CO_2-laser peak amplitude versus the driving amplitude applied to the acousto-optical modulator, presented in the right panel in Fig. 4.13.

It should be noted that the same approach can be applied to detect not only stable but also unstable orbits. Indeed, using this technique, unstable periodic orbits have been found in a loss-modulated CO_2 laser [65].

4.3.3 Bistability Induced by Resonant Perturbations

Chizhevsky et al. [59] discovered that similar to other dynamical systems (see Sect. 2.2.7), bistability can be induced by additional resonant perturbation. It was found that in a loss-modulated CO_2 laser the addition of another modulation at a subharmonic frequency of the driving loss modulation splits the bifurcation diagram into two diagrams shifted in different directions with respect to the driving amplitude which is used as a control parameter.

The double-frequency modulation is applied to the cavity loss in Eq. 4.3 as

$$k(t) = k_0 + k_d \cos(2\pi f_d t) + k_p \cos(2\pi \frac{f_d}{n} t + \phi),$$

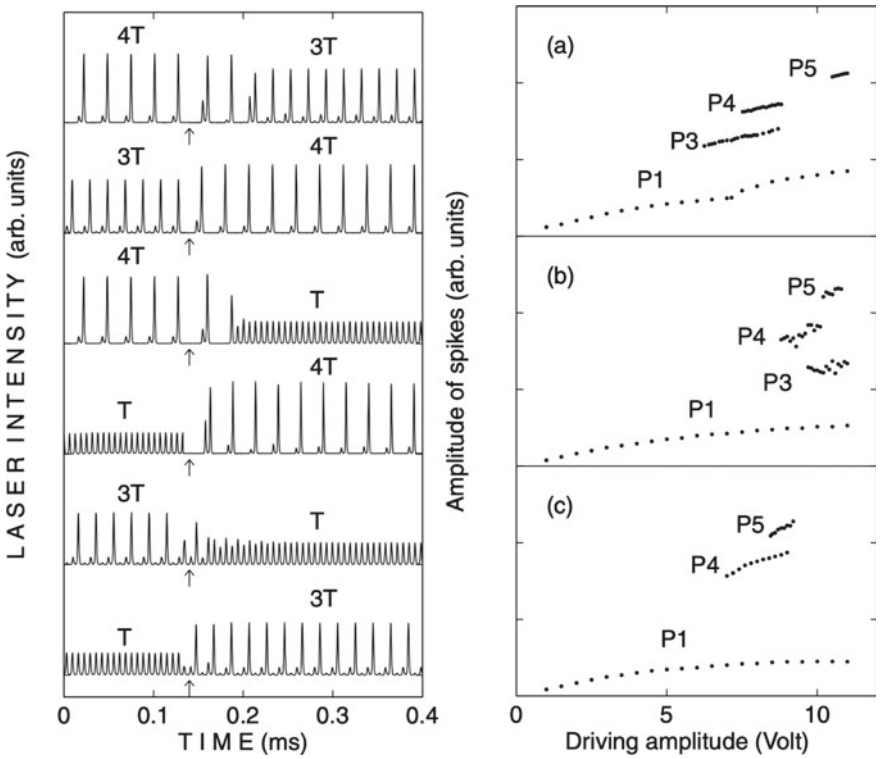

Fig. 4.13 (Left) Experimental time series showing switches between coexisting periodic orbits and (right) bifurcation diagrams of the peak laser intensity as a function of the driving amplitude applied to the loss modulator, showing the coexisting branches of periodic orbits P1, P3, P4, and P5, for modulation frequencies **a** 150, **b** 170, and **c** 180 kHz. Reprinted by permission from IOP Publishing [64]

where k_p is the perturbation amplitude at subharmonic frequency f_d/n ($n = 3, 4, 8, 16$) and ϕ is the perturbation phase.

The bifurcation diagram of the peak laser intensity with respect to the control parameter $\mu = k_d/k_{1/2}$ ($k_{1/2}$ being the first period-doubling bifurcation in the absence of the resonant perturbation) for the parameters $\tau = 3.5 \times 10^{-9}$ s, $\gamma = 1.978 \times 10^5$ s^{-1}, $y_0 = 0.175$, $k_0 = 0.1731$, $f_d = 129$ kHz, $k_{1/2} = 4.76 \times 10^{-3}$, and $\phi = 0$.

A common feature of periodically driven nonlinear systems, apart from a period-doubling route to chaos, is the presence of n subharmonic isolated branches called *isolas*, which are born in saddle-node bifurcations of the period n. For example, in the bifurcation diagram shown in Fig. 4.14, the laser parameters are chosen so that for $\mu > 2.308$ the period-2 (P2) and period-3 (P3) orbits coexist in the absence of the resonant perturbation. The addition of the resonant perturbation at $f_d/3$ splits the primary period-3 attractor into three different P3 attractors, which appear in saddle-node bifurcations at $\mu_1 = 2.236$, $\mu_2 = 2.310$, and $\mu_3 = 2.388$.

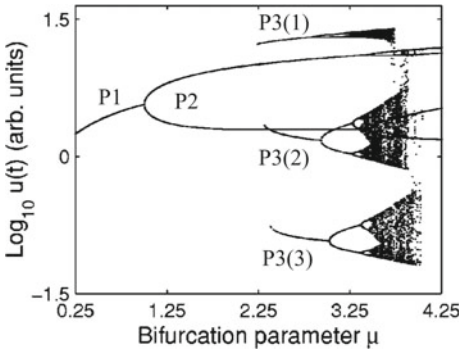

Fig. 4.14 Bifurcation diagram of log of the peak intensity of the loss-driven CO_2 laser under resonant perturbation at $f_d/3$ versus control parameter μ showing the splitting of the primary period-3 attractor into three period-3 attractors denoted by P3(1), P3(2), and P3(3). Reprinted figure with permission from [66] ©2001 by the American Physical Society

The splitting of attractors was experimentally confirmed using the experimental setup similar to that presented in Fig. 4.12, which allowed switching between the attractors [66].

4.3.4 Bistability Induced by a Delayed Feedback

A CO_2 laser with feedback is a complex system extensively studied both experimentally and numerically. As distinct from a loss-modulated CO_2 laser which can be described by the simplest two-level model in Eq. 4.3 (see Sect. 4.3.1), the CO_2 laser with feedback is modeled by either three [67] or six rate equations given as [68, 69]

$$\begin{aligned}
\dot{x}_1 &= k_0 x_1 \left\{ x_2 - 1 - k_1 \sin^2 \left[\epsilon x_6(\theta - T_0) + (1-\epsilon) x_6 \right] \right\}, \\
\dot{x}_2 &= -\Gamma_1 x_2 - 2k_0 x_1 x_2 + \gamma x_3 + x_4 + P, \\
\dot{x}_3 &= -\Gamma_1 x_3 + x_5 + \gamma x_2 + P, \\
\dot{x}_4 &= -\Gamma_2 x_4 + \gamma x_5 + z x_2 + zP, \\
\dot{x}_5 &= -\Gamma_2 x_5 + z x_3 + \gamma x_4 + zP, \\
\dot{x}_6 &= \beta \left(B - x_6 - \frac{R x_1}{1 + \alpha x_1} \right),
\end{aligned} \tag{4.5}$$

where x_1 is the normalized photon number proportional to the laser intensity, x_2 is proportional to the population inversion, x_3 is proportional to the sum of populations on the two resonant lasing levels, x_4 and x_5 are proportional, respectively, to the difference and sum of populations of the rotational manifolds coupled to the lasing levels, and x_6 is proportional to the feedback voltage that affects cavity

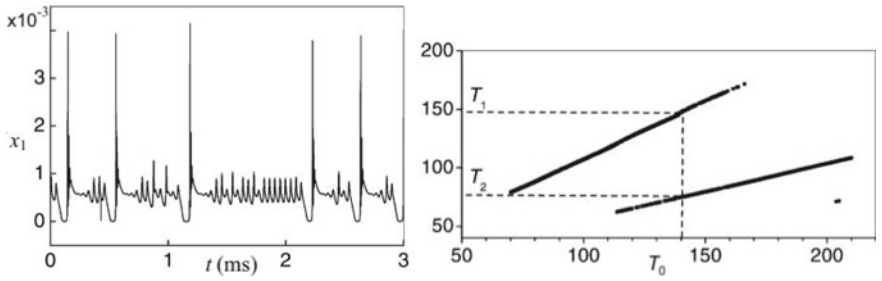

Fig. 4.15 (Left) Chaos in a CO_2 laser without delay. (Right) Periodicity of periodic orbits as a function of feedback delay T_0. The horizontal dashed lines indicate periods of coexisting orbits $T_1 = 147.3$ and $T_2 = 74.7$ at delay time $T_0 = 140$ shown by the vertical dashed line. The parameters are $\Gamma_1 = 10.0643$, $\Gamma_2 = 1.0643$, $\alpha = 32.8767$, $\beta = 0.4286$, $k_0 = 28.5714$, $k_1 = 4.5556$, $z = 10$, $\gamma = 0.05$, $R = 160$, $B = 0.10315$, and $P = 0.016$, $\epsilon = 0.25$

losses. The parameter k_0 is related to the unperturbed cavity loss, k_1 determines the modulation strength, γ is a constant regulated the coupling between the variables (x_2, x_3, x_4, x_5) and (x_3, x_2, x_5, x_4), Γ_1 and Γ_2 are decay rates of the lasing levels, P is the pump parameter, z is the effective number of rotational levels, α, β, B, and R are proportional to the saturation factor, bandwidth, bias voltage, and feedback gain, respectively. The delay term $\epsilon x_6(\theta - T_0)$ in Eq. 4.5 contains strength ϵ of the delay signal, delay time T_0, and time $\theta = t\gamma_r$ (t being the real time) rescaled to collision relaxation rate $\gamma_r = 7 \times 10^5\ \mathrm{s}^{-1}$.

Martínez-Zérega et al. [70] have found that feedback with certain delay times T_0 converts chaos in a CO_2 laser (Fig. 4.15 (left)) into coexisting periodic orbits (Fig. 4.15 (right)), whose periodicity is a linear function of the delay time T_0. As seen from the figure, bistability exists in the range of delay times $T_0 \in (110, 170)$ (in normalized units of γ_r). Note, that the periods of the two coexisting orbits are close to T_0 and $T_0/2$.

4.4 Multistability in Semiconductor Lasers

Semiconductor lasers, due to their relatively small size, low cost, and ease of operation, have a wide range of applications, from optical communication to high-speed modulation and detection. They are essentially stable devices which belong to class-B lasers and described by a set of differential equations for the complex field and the carrier density. However, it is only true for narrow-stripe edge-emitting lasers which can easily be destabilized by external perturbations, such as optical self-feedback or optical injection. Similar to other class-B lasers, semiconductor lasers can also exhibit the coexistence of multiple attractors, so that their dynamics strongly depends on initial conditions. This was demonstrated in many theoretical and experimental studies [9, 71–73].

It should noted that some semiconductor lasers have an additional degree of freedom in the device structure. For example, vertical-cavity surface-emitting semiconductor lasers (VCSEL) have a disk structure of the laser cavity larger than the optical wavelength, and therefore exhibit instabilities even in their solitary oscillations. The spatial dependence of the device structure is an additional degree of freedom beside of the structure of narrow-stripe edge-emitting semiconductor lasers. This additional degree of freedom makes possible a special type of multistability called *polarization multistability* (see Sect. 4.2.3).

Below, we will present two examples which demonstrate how the coexistence of fixed points and periodic orbits arise in semiconductor lasers. In the first example, we will describe a semiconductor laser with an external cavity, and in the second example we will consider a semiconductor laser with modulated pump current.

4.4.1 Semiconductor Laser with Delayed Feedback

In Sect. 2.2.5 we have shown that feedback can induce multistability in a dynamical system. Here, we will show that with appropriate optical feedback and certain parameters a semiconductor laser exhibits the coexistence of several fixed points. Such a behavior was first demonstrated by Masoller and Abraham [71] by numerical simulations of the Lang–Kobayashi model [74] for a single-mode semiconductor laser with weak optical feedback, given by

$$\begin{aligned} \dot{E} &= k(1+i\alpha)\left(\frac{N}{1+\epsilon|E|^2}-1\right)E+\gamma E(t-\tau)e^{-i\omega_0\tau}, \\ \dot{N} &= \frac{1}{\tau_n}\left(j-N-\frac{N|E|^2}{1+\epsilon|E|^2}\right), \end{aligned} \tag{4.6}$$

where E is the varying complex field, N is the normalized carrier density, k is the cavity losses, a is the linewidth enhancement factor, ϵ is the gain saturation coefficient, γ is the feedback light intensity, ω_0 is the optical frequency without feedback, j is the normalized injection current, τ is the round-trip time in the external cavity, and τ_n is the carrier lifetime.

While without feedback ($\gamma = 0$) the laser operates in a monostable continuous wave regime, a weak feedback induces an additional fixed point attractor, and as the feedback strength is increased, each of the coexisting states undergoes a quasiperiodic route to chaos. Two frequencies appear on this route. One of them is the relaxation oscillation frequency of the laser itself, and another one is the frequency of the external cavity (around $1/\tau$). As γ is further increased, several chaotic attractors appear for the same parameter values.

The coexistence of five chaotic attractors is shown in Fig. 4.16a in the $(\Delta\phi, |E|^2)$ plane, where $\Delta\phi = \phi(t) - \phi(t-\tau)$. The time series of variables $\Delta\phi(t)$ and $|E(t)|^2$ in one of the coexisting chaotic regimes are illustrated in Fig. 4.16b,c.

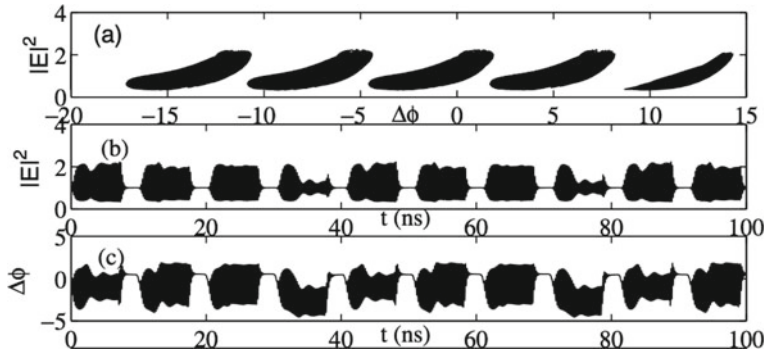

Fig. 4.16 **a** Five chaotic attractors in a semiconductor laser with delayed feedback in the $(\Delta\phi, |E|^2)$ space. **b,c** Time series of variables $\Delta\phi(t)$ and $|E(t)|^2$ in the middle chaotic attractor in (**a**). Numerical simulations were performed using Eq. 4.6 with $k = 500\,\text{ns}^{-1}$, $\epsilon = 0.003$, $\tau_n = 1$ ns, $\alpha = 3$, $j = 2$, $\omega_0\tau = 6$ rad, $\gamma = 2\ \text{ns}^{-1}$, and $\tau = 10$ ns. Reprinted figure with permission from [75] ©2002 by the American Physical Society

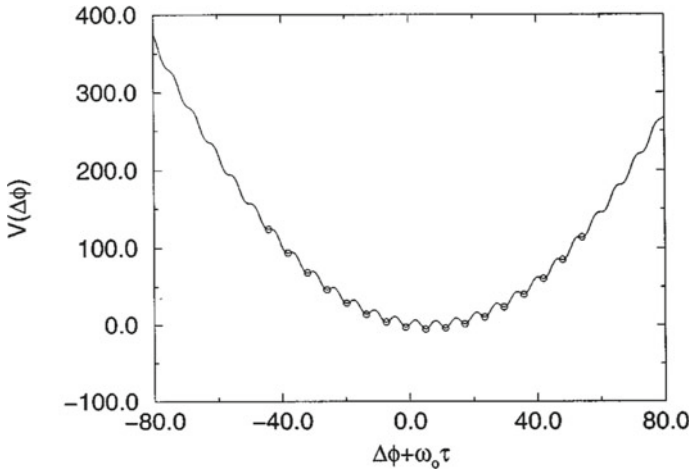

Fig. 4.17 Potential given by Eq. 4.7 of a semiconductor laser with external cavity $\gamma = 1.2 \times 10^9\ \text{s}^{-1}$, $\tau = 10$ ns, $\alpha = 4.4$, and $\omega_0\tau = 6$. The circles indicate fixed point positions. Reprinted figure with permission from [71] ©1998 by the American Physical Society

Dynamics of the semiconductor laser with external cavity is governed by the potential given by

$$V(\Delta\phi) = \Delta^2\phi/2\tau - \gamma\sqrt{1+\alpha^2}\cos(\Delta\phi + \omega_0\tau + \arctan\alpha) \tag{4.7}$$

and depicted in Fig. 4.17. For the selected parameter values the potential displays 17 coexisting fixed points.

4.4.2 Directly Modulated Semiconductor Laser

A unique feature of semiconductor lasers is that, unlike other externally modulated lasers, a laser diode can be directly modulated by changing the injection current. This is especially important in view of the possibility of monolithic laser integration and modulation of electronic circuits. High-speed direct modulation in these lasers opens up great opportunities for the development of high-capacity information transfer and ultrafast optical processing systems.

It is now widely accepted that a single-mode semiconductor laser can evolve to chaos through a cascade of period-doubling bifurcations under the action of a modulation current. However, systematic experimental studies, in particular, long time series analysis, are not available because the time scale of the laser pulses is in a picosecond range. Much progress in understanding the origin of bifurcations was achieved through numerical simulations with simple models.

The dynamics of a single-mode semiconductor laser with direct pump current modulation [76] can be described by two evolution equations, one for the photon density of the electric field inside the laser cavity (S) and the other for the carrier density (N) or the number of electron-hole pairs) [77], as follows

$$\begin{aligned} \dot{S} &= G_N(N - N_0)(1 - \epsilon S)S - \frac{S}{\tau_p} + \frac{BN}{\tau_c}, \\ \dot{N} &= j - \frac{N}{\tau_c} - G_N(N - N_0)(1 - \epsilon S)S, \end{aligned} \tag{4.8}$$

where τ_c and τ_p are the carrier and photon lifetimes, respectively, B is the spontaneous emission factor, G_N is the modal gain coefficient, N_0 is the carrier density required for the transparency of the active region, ϵ is the gain saturation coefficient, and j is the injection current density.

Under periodic modulation of the injection current

$$j = j_b + j_m \sin(2\pi\nu_m t), \tag{4.9}$$

with certain parameters of bias current density j_b, driving current density j_m, and driving frequency ν_m, the laser exhibits the coexistence of three attractors: period 1 (P1), period 3 (P3), and period 4 (P4).

The time series of three coexisting periodic orbits are presented in Fig. 4.18 for the following set of the system parameters: $\tau_p = 6 \times 10^{-12}$ s, $\tau_s = \times 10^{-9}$ s, $N_0 = 10^{24}$ m$^{-}3$, $B = 10^{-5}$, $G_N = 10^{-12}$ m^{3}s^{-1}, $\epsilon = 8 \times 10^{-24}$ m^3, $x_m = j_m/j_b = 0.6$, and $\nu_m = 2.9$ GHz.

Figure 4.19 shows the bifurcation diagrams of the peak photon density with respect to the driving frequency (left panel) and amplitude (right panel) calculated for randomly chosen initial conditions. One can see the coexistence of three periodic orbits (P1, P3, and P4) in a certain range of the control parameters.

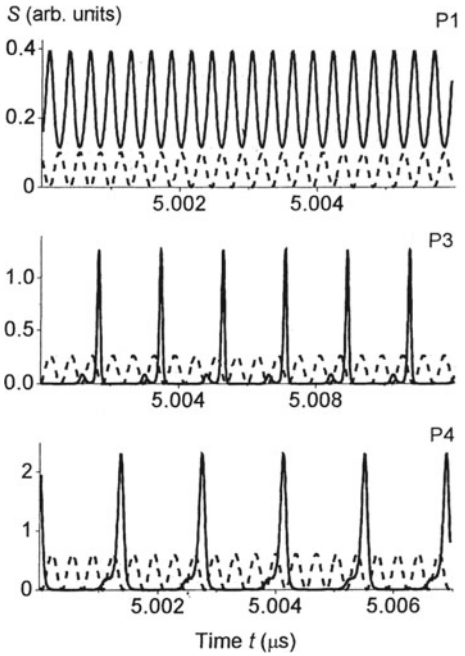

Fig. 4.18 Coexisting period-1 (P1), period-3 (P3), and period-4 (P4) regimes in a semiconductor laser model (Eq. 4.8) with direct current modulation (Eq. 4.9). The dashed lines show the driving signal

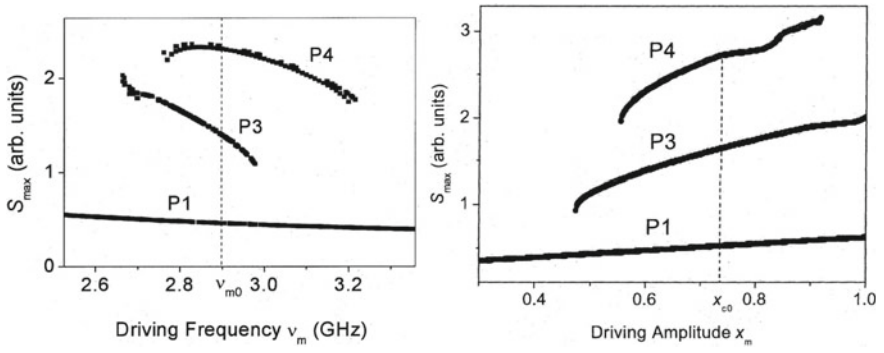

Fig. 4.19 Bifurcation diagrams of peak photon density S_{max} as a function of (left) driving frequency ν_m for the fixed driving amplitude $x_m = x_{c0} = 0.6$ and (right) driving amplitude x_m for the fixed driving frequency $\nu_m = \nu_{m0} = 2.9$ GHz

Knowing how multistability arises, one can begin to manage it. In particular, coexisting attractors can be selectively destroyed by adding harmonic parametric modulation with a frequency an order of magnitude lower than the excitation frequency [76]. Such control provides more flexibility in manipulating the laser dynamics to select the desired behavior, and this technique works well even when both driving and control are applied to the same laser parameter. Optimal control conditions are achieved when the control frequency is close to the relaxation oscillation frequency of the attractor we want to annihilate.

4.5 Multistability in Fiber Lasers

Multistability in fiber lasers has perhaps been studied more extensively than in other types of lasers, particularly, in an erbium-doped fiber laser (EDFL). The interest in studying the dynamics of these lasers is due to their applications in communications, reflectometry, sensing, and medicine [78]. From the viewpoint of nonlinear dynamics, fiber lasers doped with rare earth elements belong to class-B lasers. These are nonautonomous systems in which polarization is adiabatically eliminated and the dynamics can be described by two rate equations for field and population inversion. However, under loss or pump modulation these lasers can exhibit complex dynamical behavior including the coexistence of various attractors.

The dynamics of a single-mode EDFL is described by the following rate equation model [79]

$$\begin{aligned} \dot{P} &= \frac{2L}{T_r} P \left\{ \tau_w \alpha_0 \left[N(\xi_1 - \xi_2) - 1 \right] - \alpha_{th} \right\} + P_{sp}, \\ \dot{N} &= -\frac{\sigma_{12} r_w P}{\pi r_0^2} (N\xi_1 - 1) - \frac{1}{\tau} + P_{pump}, \end{aligned} \tag{4.10}$$

where P is the intracavity laser power, $N = (1/n_0 L) \int_0^L N_2(z) dz$ is the averaged (over the active fiber length L) population of the upper lasing level, N_2 is the upper level population at the z coordinate, n_0 is the refractive index of a "cold" erbium-doped fiber core, ξ_1 and ξ_2 are parameters defined by the relationship between cross-section of ground state absorption σ_{12}, return stimulated transition σ_{21}, and excited state absorption σ_{23}, T_r is the photon intracavity round-trip time, α_0 is the small-signal absorption of the erbium fiber at the laser wavelength, α_{th} is the intracavity loss on the threshold, τ is the lifetime of erbium ions in the excited state, r_0 is the fiber core radius, w_0 is the radius of the fundamental fiber mode, and r_w is the factor addressing a match between the laser fundamental mode and erbium-doped core volumes inside the active fiber. The spontaneous emission into the fundamental laser mode P_{sp} and pump power P_{pump} are given as

$$
\begin{aligned}
P_{sp} &= N\frac{10^{-3}}{\tau T_r}\left(\frac{\lambda_g}{w_0}\right)^2 \frac{r_0^2\alpha_0 L}{4\pi^2\sigma_{12}},\\
P_{pump} &= P_p\frac{1-\exp\left[-\alpha_0\beta L(1-N)\right]}{N_0\pi r_0^2 L},
\end{aligned}
\tag{4.11}
$$

where λ_g is the laser wavelength, P_p is the pump power at the fiber entrance and β is a dimensionless coefficient. The parameters are chosen so to correspond to real experimental conditions: $L = 0.88$ m, $T_r = 8.7$ ns, $r_w = 0.308$, $\alpha_0 = 40\ \mathrm{m}^{-1}$, $\xi_1 = 2$, $\xi_2 = 0.4$, $\alpha_{th} = 3.92 \times 10^{-2}$, $\sigma_{12} = 2.3 \times 10^{-17}\ \mathrm{m}^2$, $r_0 = 2.7 \times 10^{-6}$ m, $\tau = 10^{-2}$ s, $\lambda_g = 1.65 \times 10^{-6}$ m, $w_0 = 3.5 \times 10^{-6}$ m, $\beta = 0.5$, and $N_0 = 5.4 \times 10^{25}\ \mathrm{m}^{-3}$.

For simplicity, the system given by Eq. 4.10 can be transformed into the simple normalized form

$$
\begin{aligned}
\frac{dx}{d\theta} &= xy - a_1 x + a_2 y + a_3,\\
\frac{dy}{d\theta} &= c - xy - b_1 y - b_2 + P_0(1 - b_3 e^y),
\end{aligned}
\tag{4.12}
$$

where x and y are the normalized laser power density and inversion population, respectively, θ, a_1, and P_0 are proportional to time, cavity loss, and pump power.

Below, we will describe the EDFL dynamics under periodic modulation of the cavity losses L and pump parameter P.

4.5.1 Loss-Modulated Fiber Laser

We consider first the EDFL in Eq. 4.10 under cavity loss modulation given by

$$
L = L_0\left[1 + L_m \sin(2\pi f t)\right], \tag{4.13}
$$

where L_m and f are the modulation depth and frequency, respectively, and L_0 is the constant loss without modulation (at $L_m = 0$). In the normalized form, Eq. 4.13 is equivalent to the modulation of the parameter a_1 in the normalized Eq. 4.12 as follows

$$
a_1 = a_0 + a_m \sin(2\pi\nu\theta), \tag{4.14}
$$

where a_0, a_m, and ν are proportional to the constant cavity loss, modulation depth and frequency, respectively.

The loss-modulated EDFL exhibits the coexistence of periodic orbits for a certain parameter range, as shown in the bifurcation diagram in Fig. 4.20 obtained using random initial conditions. When the modulation amplitude is small, the regular period-1 attractor (R1) coexists with the period-2 attractor (P2) which is born in a saddle-node bifurcation. An increase in the modulation depth enriches the laser

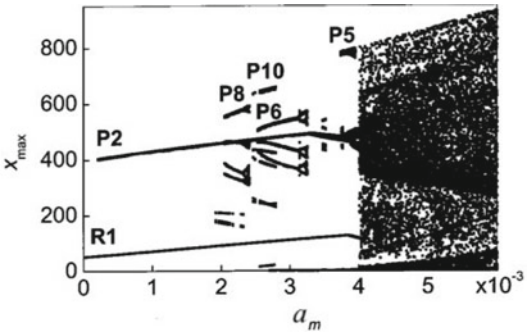

Fig. 4.20 Bifurcation diagram of local maxima of normalized photon density versus loss-modulation depth a_m in EDFL with frequency $\nu = 2.2 \times 10^3$. The letters and numbers indicate orbit periods corresponding to different attractors obtained using random initial conditions

dynamics by inducing various bifurcations (periods 8, 10, 6, etc.) which give rise to other periodic attractors that appear in corresponding primary saddle-node bifurcations. All these periodic orbits undergo a cascades of period-doubling bifurcations and finally are simultaneously destroyed with their basins of attraction in boundary crisis.[1]

A similar behavior was observed in a driven CO_2 laser [81]. Regular saddles emanating from primary saddle-node bifurcations play a significant role in the emergence of this kind of crisis.

Another type of crisis arises at $a_m \approx 4 \times 10^{-3}$, where a sudden expansion of the chaotic attractor occurs between all branches developing from the primary saddle-node bifurcation giving rise to a period 5 (P5) attractor. Then, the trajectory visits phase space regions which were previously outside the attractor. Such a sudden increase of the chaotic attractor in size occurs when the periodic orbit with which the chaotic attractor collides, is inside its basin, and called *interior crisis* [82]. This kind of crisis was also observed in a loss-modulated CO_2 laser (see Fig. 4.11).

An increase in the modulation amplitude a_m enriches the dynamics of the loss-modulated EDFL, as seen from Fig. 4.21. When a_m is very small, the laser behaves as a harmonic oscillator and responds linearly to external modulation with a resonance at the relaxation oscillation frequency ν_r (Fig. 4.21a). For larger modulation amplitudes, nonlinearity becomes relevant that gives rise to bistability which can be revealed through a hysteresis. R1 and P1 branches of attractors are born and dead in saddle-node bifurcations S_1 and S_2, respectively, and coexist in the range of $\nu \in (1.1, 1.5) \times 10^3$, as well as P1 and P2 branches coexist in the range of $\nu \in (2.50, 3.05) \times 10^3$. The latter range is located around the second harmonic of ν_r. Due to nonlinearity, the maxima of two stable period-1 branches (P1 and R1) are not located anymore at the relaxation oscillation frequency ν_r, but shifted towards smaller frequencies $\nu(S_1) \approx 1.1 \times 10^3$ and $\nu(S_2) \approx 1.5 \times 10^3$. These stable branches are connected by the unstable period-1 branch (shown by crosses). Such saddle-node bifurcations are interesting, but difficult to find, since the maximum response in both branches

[1] A crisis is a sudden change in the attractor behavior due to a collision of an unstable periodic orbit with a chaotic attractor. When the orbit is just at the boundary of the basin of attraction of the chaotic attractor, the crisis is called *boundary crisis* [80].

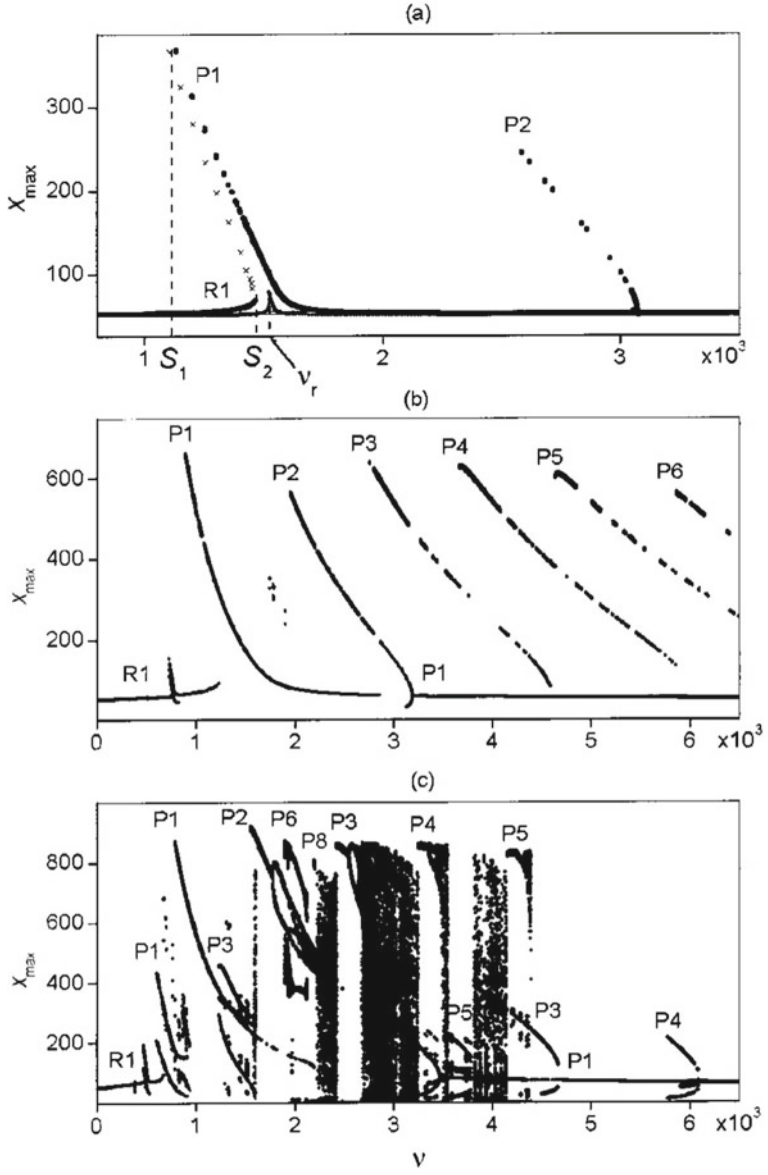

Fig. 4.21 Bifurcation diagrams of EDFL peak density versus modulation frequency at different modulation depths: **a** $a_m = 10^{-5}, 10^{-4}$, **b** 10^{-3}, and **c** 4×10^{-3}. The crosses mark unstable period-1 solutions, S_1 and S_2 indicate supercritical and subcritical period-1 saddle-node bifurcations, and ν_r is the relaxation oscillation frequency. Reprinted with permission from [11] ©2003 The Optical Society

appears just before the solutions become unstable. Similar hysteresis behavior was also observed in pump-modulated [72] and loss-modulated semiconductor lasers (see Sect. 4.4), as well as in a pump-modulated ring EDFL [83].

At high modulation amplitudes (see Fig. 4.21b, c), the laser dynamics becomes more complicated and multistability arises. In addition, primary attractors (P2, P3, P4, P5) undergo period-doubling bifurcations, as the control parameter ν is increased, followed by the Feigenbaum transition to chaos and ending with crisis.

4.5.2 *Pump-Modulated Fiber Laser*

Next, we will show how multistability arises in an EDFL under diode pumped current modulation. It should be noted that the experimental implementation of pump modulation is much easier than that of the loss modulation because the former can be achieved by the direct modulation of a diode pump laser current as follows

$$P_p = p\,[1 - m\sin(2\pi f_d t)]\,, \tag{4.15}$$

where m and f_d are the modulation depth and frequency, respectively, and p is the constant pump power without modulation.

The EDFL under pump modulation displays very rich dynamics. The coexistence of up to four periodic orbits (P1, P3, P4, P5) is observed, as seen in the bifurcation diagrams of the peak laser power with respect to the modulation frequency and amplitude in Fig. 4.22. Similarly to the loss modulation case (see Sect. 4.5.1), stable

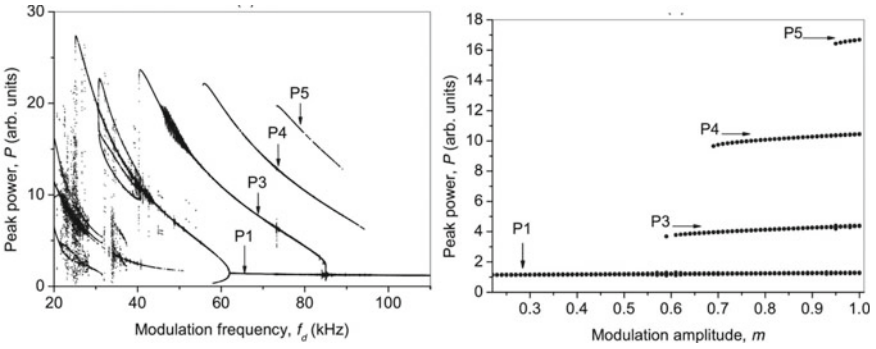

Fig. 4.22 Bifurcation diagrams of EDFL peak power versus (left) driving frequency f_d for $m = 1$ and (right) driving amplitude m with frequency $f_d = 80$ kHz. The diagrams are calculated by random varying initial conditions and using the continuation method. The arrows indicate branches of the coexisting P1, P3, P4, and P5 orbits. Reprinted figure with permission from [84] ©2012 by the American Physical Society

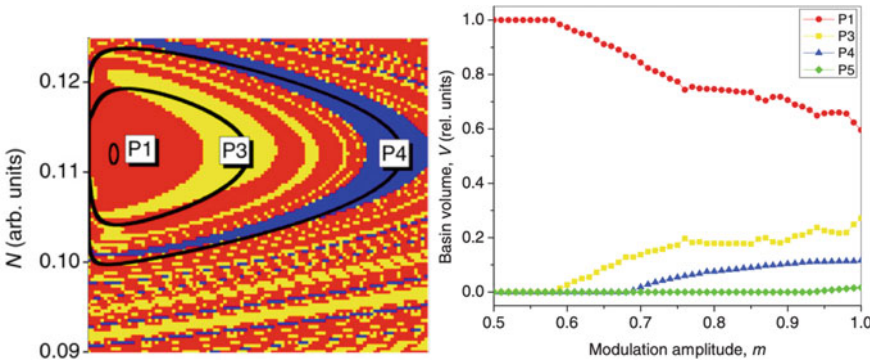

Fig. 4.23 (Left) Basins of attraction of four coexisting periodic orbits in the EDFL under pump modulation with $f_d = 70.2$ kHz and $m = 0.8$. P1, P3, and P4 are shown, respectively, by red, yellow, and blue dots. The corresponding periodic orbits are marked by black lines. (Right) Relative basin volumes of coexisting periodic orbits versus driving amplitude with frequency $f_d = 80$ kHz

periodic orbits on subharmonic frequencies (P3, P4, and P5) are born in saddle-node bifurcations when the control parameter is increased (compare with Figs. 4.20 and 4.21).

In the left panel in Fig. 4.23 we plot the basins of attraction of the coexisting stable periodic orbits. One can see that the basins have Wada properties (see Sect. 1.2.4). The basin volumes shown in the right panel in Fig. 4.23 depend on the modulation amplitude. Note that for low modulation amplitudes ($m < 0.57$) the laser is monostable with a single P1. However, as m is increased, the subharmonic attractors of P3 and P4 emerge, and their basins of attraction enlarge, while the P1 basin volume decreases. Finally, at $m = 0.93$ the P5 attractor arises, so that five attractors coexist.

Laser experiments confirm the coexistence of various attractors in the EDFL. The experimentally obtained bifurcation diagrams with respect to the modulation frequency and amplitude are presented in Fig. 4.24. Due to experimental noise, the attractor branches are broadened.

The comparison of Figs. 4.22 and 4.24 displays a very good agreement between the numerical and experimental results that indicates the adequacy of the used theoretical model in Eq. 4.10. In addition, the model demonstrates a fundamental understanding of the laser dynamics and gives us an idea of the origin of non-trivial experimentally observable effects such as extreme events (see Sect. 5.5.3) and noise-induced preference for certain states (see Sect. 5.5). Due to the uncontrollability of internal laser noise, extreme pulses in the experiment appear at lower amplitudes of external noise than in numerical simulations.

Finally, the preference for certain states in multistate intermittency depends nonmonotonically on the noise amplitude. This means that there is a certain level of noise for which a certain state is more likely than for other noise amplitudes. This result agrees with the previously observed effect of nonmonotonic preference of attractors observed in the multistable Hénon map [85].

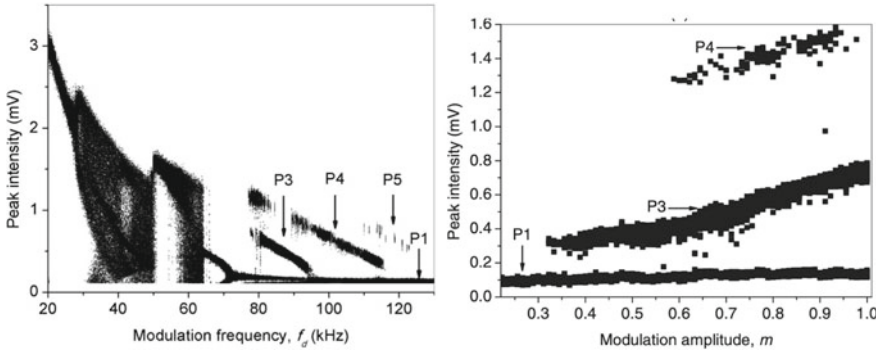

Fig. 4.24 Experimental bifurcation diagrams of laser peak intensity versus (left) driving frequency for $m = 0.8$ and (right) driving amplitude for $f_d = 90$ kHz. The diagrams are calculated by switching on and off the signal generator. The arrows indicate the branches of the coexisting P1, P3, P4, and P5 periodic orbits. Reprinted figure with permission from [84] ©2012 by the American Physical Society

References

1. Szöke A, Daneu V, Goldhar S, Kurnit NA (1969) Bistable optical element and its applications. Appl Phys Lett 15(11):376–379
2. Gibbs HM, Mo Call SL, Venkatesan TNC (1976) Differential gain and bistability using a sodium-filled Fabry-Perot interferometry. Phys Rev Lett 36(11):1135–1138
3. Grazyuk AZ, Oraevsky AN (1964) Transient processes in a molecular generator. Radiotekhnika i Elektronika 9(3):524–532
4. Arecchi FT, Meucci R, Puccioni G, Tredicce J (1982) Experimental evidence of subharmonic bifurcations, multistability, and turbulence in a Q-switched gas laser. Phys Rev Lett 49:1217–1220
5. Weiss CO, Godone A, Olafsson A (1983) Routes to chaotic emission in a cw He-Ne laser. Phys Rev A 28(2):892–895
6. Brun E, Derighetti B, Meier D, Holzner R, Ravani M (1985) Observation of order and chaos in a nuclear spin-flip laser. J Opt Soc Am B 2:156–167
7. Baer T (1986) Large-amplitude fluctuations due to longitudinal mode coupling in diode-laser pumped intracavity-doubled Nd:YAG lasers. J Opt Soc Am B 3:1175–1180
8. de Jagher PC, van der Graaf WA, Lenstra D (1996) Relaxation-oscillation phenomena in an injection-locked semiconductor laser. Quant Semiclass Opt 8:805–822
9. Gavrielides A, Kovanis V, Varangis PM, Erneux T, Lythez G (1997) Coexisting periodic attractors in injection-locked diode lasers. Quant Semiclass Opt 9:785–796
10. Pisarchik AN, Barmenkov YO, Kir'yanov AV (2003) Experimental characterization of bifurcation structure in an erbium-doped fiber laser with pump modulation. IEEE J Quantum Electron 39:1567–1571
11. Saucedo-Solorio JM, Pisarchik AN, Kir'yanov AV, Aboites V (2003) Generalized multistability in a fiber laser with modulated losses. J Opt Soc Am B 20:490–496
12. Pisarchik AN, Feudel U (2014) Control of multistability. Phys Rep 540:167–218
13. Brambilla M, Lugiato LA, Penna V, Prati F, Tamm C, Weiss C (1991) Transverse laser patters. II. Variational principle for pattern selection, spatial multistability and laser hydrodynamics. Phys Rev A 43:5114–5120
14. Pampaloni E, Residor S, Soria S, Arecchi F (1997) Phase-locking in nonlinear optical patterns. Phys Rev Lett 78:1042–1045